



Cite this: *Soft Matter*, 2016, 12, 6964

Both monovalent cations and plectin are potent modulators of mechanical properties of keratin K8/K18 networks†

I. Martin,^{*a} M. Moch,^{bf} T. Neckernuss,^a S. Paschke,^c H. Herrmann^{de} and O. Marti^a

Intermediate filament (IF) networks are a major contributor to cell rigidity and thus serve as vital elements to preserve the integrity of entire cell layers. Keratin K8 and K18 IFs are the basic constituents of the cytoskeleton of epithelial cells. The mechanical properties of K8/K18 networks depend on the structural arrangements of individual filaments within the network. This paper investigates the architecture of these networks *in vitro* under the influence of the monovalent cation potassium and that of the cytolinker protein plectin. Whereas increasing amounts of potassium ions lead to filament bundling, plectin interlinks filaments at filament intersection points but does not lead to bundle formation. The mechanics of the resulting networks are investigated by microrheology with assembled K8/K18 networks. It is shown that bundling induced by potassium ions significantly stiffens the network. Furthermore, our measurements reveal an increase in plectin-mediated keratin network rigidity as soon as an amount corresponding to more than 20% of the plectin present in cells is added to the keratin IF networks. In parallel, we investigated the influence of plectin on cell rigidity in detergent-extracted epithelial vulva carcinoma derived A431 cells *in situ*. These cytoskeletons, containing mostly IFs, actin filaments and associated proteins, exhibit a significantly decreased stiffness, when plectin is downregulated to $\approx 10\%$ of the normal value. Therefore, we assume that plectin, *via* the formation of IF–IF connections and crosslinking of IFs to actin filaments, is an important contributor to cell stiffness.

Received 25th April 2016,
Accepted 25th July 2016

DOI: 10.1039/c6sm00977h

www.rsc.org/softmatter

Introduction

Intermediate filaments (IFs) constitute, together with actin filaments and microtubules, the cytoskeleton of metazoan cells. They form a composite network of semiflexible filaments responsible for the mechanical integrity of cells.¹ To adapt to the requirements of different tissues, IFs share a very versatile structure, encoded by approximately 70 genes in humans.²

Even though the primary amino acid sequence varies considerably,³ subunits of all IFs are dimers of fibrous proteins consisting of a central α -helical “rod” domain able to form a coiled coil, flanked by flexible “head” and “tail” domains.⁴ In the case of keratins, a special subgroup of IF proteins,

heterodimers are formed from one monomer each of the basic and the acidic subgroup.⁵ These dimers anneal laterally to half-staggered, anti-parallel tetramers, which associate further to unit-length filaments (ULFs) and then elongate longitudinally to long filaments.^{6–10} While the head domains are important for longitudinal annealing, truncation of the highly charged tail domains does not inhibit filament formation. Tail domains play a role in lateral interactions with neighboring filaments *via* counterions and in controlling the diameter of IFs.¹¹

Intermediate filaments in cells are interconnected with each other as well as with other cytoskeletal components by cross-linking proteins, so-called cytolinkers, and ions. Typical cytolinkers are plectin, desmoplakin and epiplakin,¹² while ions abundant in cells are for example potassium and magnesium. The physiological concentration of magnesium ($0.2\text{--}0.6\text{ mM}^{13}$) and potassium ($\leq 140\text{ mM}^{14,15}$) varies according to the cell type.

IF proteins are highly charged, the net charge being negative for nearly every representative. For example, keratin K8/K18 carries a line charge of $-3\text{ e}^- \text{ nm}^{-1}$.¹⁶ Thus, positively charged ions lead to bundling. This was observed for vimentin and keratin, although keratin already shows bundle formation with monovalent ions,¹⁶ while for vimentin divalent ions are needed.^{17,18}

In this work we investigate the influence of monovalent ions by using KCl and of plectin on keratin network morphology

^a Institute of Experimental Physics, Ulm University, 89081 Ulm, Germany.
E-mail: navi.exphys@uni-ulm.de

^b Department of Internal Medicine I, Ulm University, 89081 Ulm, Germany

^c Department of General and Visceral Surgery, Ulm University, 89081 Ulm, Germany

^d Division Molecular Genetics, German Cancer Research Center (DKFZ), 69120 Heidelberg, Germany

^e Institute of Neuropathology, University Hospital Erlangen, 91054 Erlangen, Germany

^f Institute of Molecular and Cellular Anatomy, RWTH Aachen University, 52057 Aachen, Germany

† Electronic supplementary information (ESI) available. See DOI: 10.1039/c6sm00977h

with scanning electron microscopy (SEM). Furthermore, the impact on mechanical properties is examined by applying passive microrheology. Experiments are performed on *in vitro* assembled keratin K8/K18 networks, because in this system changes in sample preparation can be directly related to changes in measured properties. In the cellular situation, downregulation of a certain protein might lead to the upregulation of another factor to compensate for the loss. Nevertheless, for plectin, the *in vitro* results are directly compared to extracted networks from A431 cell clones. In these single cell

clones plectin is stably downregulated *via* shRNA by $\approx 90\%$ and the elasticity is compared to that of cells transduced with scramble control shRNA.

Results

Effect of KCl on *in vitro* assembled K8/K18 networks

Assembly of keratin K8/K18 *in vitro* results in entangled networks where single filaments are interwoven with each other,

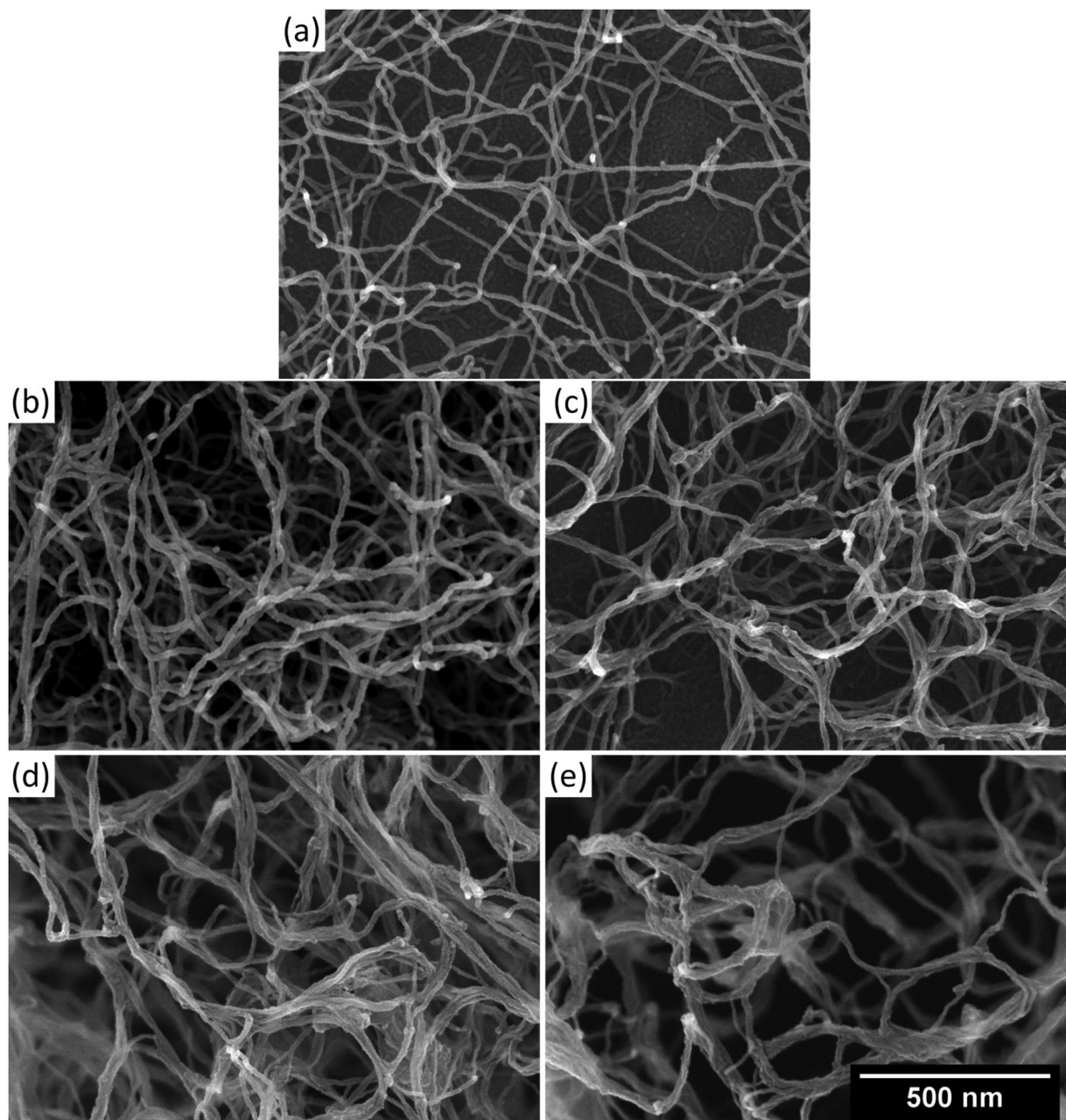


Fig. 1 SEM images of *in vitro* assembled K8/K18 networks with different concentrations of KCl. (a) No KCl, (b) 40 mM KCl, (c) 80 mM KCl, (d) 150 mM KCl, (e) 300 mM KCl. Without KCl individual filaments are partially stretched and partially corrugated and no bundles are present. With increasing ion concentration, the filaments gradually align in parallel, form bundles and decrease their spacing within bundles. Different bundles are connected through branching and subsequent recombination of one of the branching arms with neighboring bundles.

without the formation of fixed connections between them. Fig. 1(a) shows a scanning electron microscope (SEM) image of such a network. There, some filaments are stretched while others have a corrugated conformation, with a curvature depending on their persistence length. Stretched filaments are either fixed at the substrate or at connection points between filaments. These connections are probably an artifact of glutaraldehyde fixation.

When salt is added in sufficient concentrations, the assembly does not result in homogeneously distributed networks. This is unlike networks assembled without any type of salt. The networks cluster in some regions, while no IFs are left in other areas. Therefore, the networks shown in Fig. 1 appear denser for higher KCl concentrations than for lower ones. This effect was already shown by Kayser *et al.*¹⁹ Furthermore, KCl induces bundling, similar to MgCl_2 .¹⁹ In Fig. 1(b)–(e) networks with increasing concentrations of KCl are shown. Fig. 1(b) displays a network assembled with 40 mM KCl. Some filaments are aligned laterally, but no clear bundling is observed. By increasing the KCl concentration further to 80 mM (Fig. 1(c)), loose bundles can be distinguished. At approximately physiological intracellular concentrations (Fig. 1(d), 150 mM KCl) bundles increase further in density, but still individual filaments can be distinguished within bundles. With 300 mM KCl (Fig. 1(e)) bundles are so compact that single fibers can hardly be seen. These bundles divide and combine with other bundles. Sometimes even single filaments leave bundles and join others.

After the incorporation of polystyrene beads into the network, bead trajectories were measured and mean squared displacements (MSDs) were calculated. Fig. 2 shows the resulting curves

for various KCl concentrations. For better assessment of the network MSDs, the MSD of pure water is included in blue. In comparison, the MSD of K8/K18 networks without additional ions (black) is lower and displays a smaller slope, corresponding to a lower viscosity. After the addition of 5 mM KCl no alterations were observed. A further increase of the KCl concentration lowered the MSD gradually. This continues for networks assembled with up to 80 mM KCl. The MSDs for 80 and 150 mM KCl show only minor differences. Thus, even though the network morphology obviously changes (compare Fig. 1(c) and (d)), the rigidity of the network remains the same.

The general trend of all network MSDs shows decreasing slopes for larger times τ in the double logarithmic plot, which is typical for sub-diffusion. This was proven by fitting a power law and classification of the resulting diffusive exponent α between 0 and 1. No plateau can be observed in the MSD in the studied time regime.

By comparison of all MSD values of individual beads at $\tau = 0.1$ s, it was confirmed that there is no significant difference between 0 and 5 mM KCl ($p = 0.807$) and only a minor difference between 80 and 150 mM KCl ($p = 0.026$) (Wilcoxon rank-sum test). Between all other KCl concentrations there are significant differences.

The distribution of MSD values from the same lag time τ can also be used to investigate the heterogeneity of different networks. This describes how much the sample varies when measured at different positions and is therefore a measure for error bars (which are not included in Fig. 2 due to better visibility). Therefore the contribution of the highest 10% of MSD values of individual beads to the ensemble average was calculated by summation of the highest 10% of MSD values and division of the result by the sum of all values.²⁰ Using this method, completely homogeneous samples exhibit a heterogeneity of 0.1, while increasing heterogeneities lead to higher values. In our measurements we obtained approximately 0.15 for 0 mM KCl and 5 mM KCl, representing almost homogeneous samples. A further increase of the KCl concentration leads to higher heterogeneity values, with a maximum of slightly above 0.4 with 80 mM KCl. Thus, higher salt concentrations induce the formation of more heterogeneous networks.

The MSD curves were used to calculate the dynamic shear modulus and thus the storage modulus G' and the loss modulus G'' . The resulting graphs are shown in the ESI† (Fig. S1). As expected from the MSDs, both G' and G'' become higher for increasing KCl concentrations. By plotting double logarithmically all curves appear approximately linear. No minima, points of inflection or plateaus G_0 can be observed. Calculation of an estimation of G_0 ²¹ leads to the result that the plateau is at higher frequencies than accessible with our set-up.

Crossover frequencies between G' and G'' are at low frequencies in the measured regime or below the measured regime. The loss modulus G'' dominates for higher frequencies and the storage modulus G' dominates at low frequencies.

Effect of plectin on *in vitro* assembled K8/K18 networks

For *in vitro* networks assembled in the presence of plectin at first the morphology was examined with SEM. Plectin was

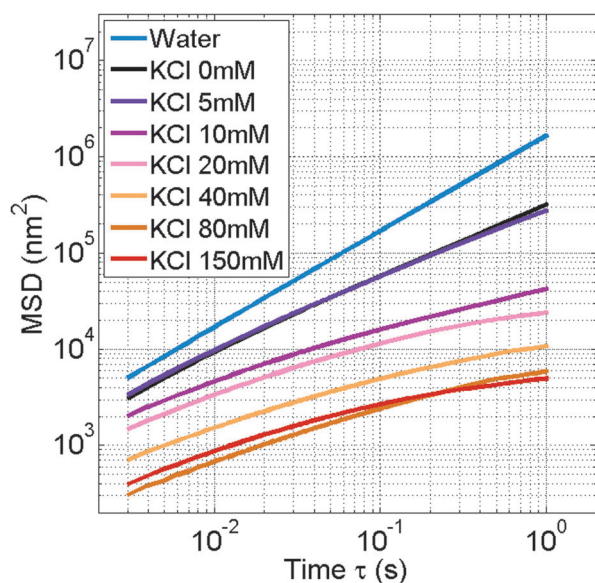


Fig. 2 MSDs of K8/K18 networks assembled with different concentrations of KCl (sampling rate 1000 Hz). The MSD of K8/K18 samples without ions is lower than that of water. Addition of KCl gradually decreases the MSD curves. The shape of the curve is typical for the sub-diffusive behaviour of visco-elastic networks. (The numbers of beads measured for each MSD are: water $n = 64$, 0 mM KCl $n = 488$, 5 mM KCl $n = 122$, 10 mM KCl $n = 140$, 20 mM KCl $n = 137$, 40 mM KCl $n = 124$, 80 mM KCl $n = 111$, 150 mM KCl $n = 131$.)

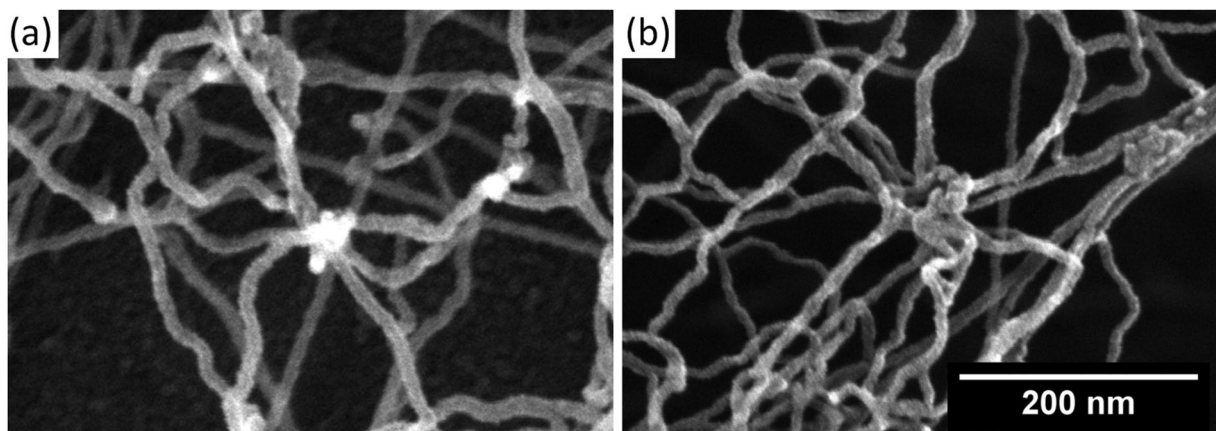


Fig. 3 SEM images of K8/K18 samples with different mass ratios of plectin/keratin (c_P/c_K). (a) $c_P/c_K = 0.12$ (b) $c_P/c_K = 0.15$. Plectin is incorporated into the network as clustered structures with different sizes, depending on the plectin concentration. The clusters interconnect IFs at specific binding points and do not induce bundling.

incorporated into the network as clusters of several plectin molecules with different shapes and sizes (Fig. 3). The presence of plectin in these clusters was confirmed by immuno-gold staining with plectin antibodies (data not shown). Similar structures have been observed previously for plectin co-assembled *in vitro* with vimentin, both purified from rat glioma C6 cells, as well as in detergent-extracted and immuno-labelled cytoskeletons of rat embryo fibroblasts.²² In Fig. 3(a) we show that the clusters interconnect IFs at filament intersection points. In between these intersection points, the filaments exhibit a similar appearance as networks without added cross-linkers (Fig. 1(a)). By increasing the plectin concentration relative to keratin, the clusters increase in abundance and become larger (compare Fig. 3(a) and (b)). They do not only interconnect two filaments but often several at once (Fig. 3(b)). Many filaments run into the complexes at different angles and positions. In contrast to potassium ions, we did not observe filament bundling at any plectin concentration employed.

To measure the influence of plectin on mechanical network properties, the physiological concentration of plectin is important. Foisner *et al.*²² described a mass ratio of plectin/vimentin of $c_P/c_V = 0.29$ in dissolved cells. In our experiments we used a keratin concentration of $c_K = 0.5 \text{ g l}^{-1}$ and added increasing concentrations of plectin to evaluate at which ratio an increase in network stiffness is achieved.

The resulting MSDs with various plectin concentrations are shown in Fig. 4. The general shape of all MSD curves is the same as for networks assembled with KCl, representing sub-diffusive behavior. It can be observed that $c_P/c_K = 0.018$ and $c_P/c_K = 0.06$ show no significant effect. The MSDs are very similar to pure keratin K8/K18 networks even though they are not identical due to limitations of the applied correction methods. $c_P/c_K = 0.12$ results in an MSD that is obviously lower than for the other network types for times larger than approximately 0.01 s. With $p = 8.4 \times 10^{-65}$ the difference between $c_P/c_K = 0$ and $c_P/c_K = 0.12$ is highly significant at $\tau = 0.1$ s. The network shown in Fig. 3(a) corresponds to this plectin concentration.

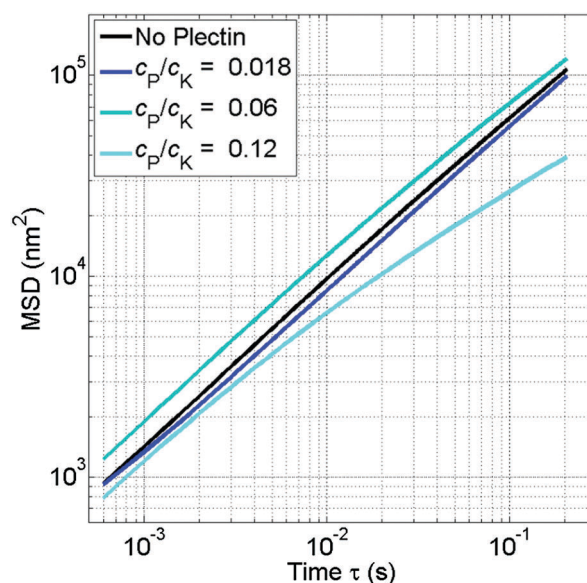


Fig. 4 MSDs of K8/K18 networks ($c_K = 0.5 \text{ g l}^{-1}$) with different concentrations of plectin (c_P) (sampling rate 5000 Hz). A ratio c_P/c_K larger than 0.06 is needed for a significant ($p = 8.4 \times 10^{-65}$) increase in network stiffness. (The numbers of beads measured for each MSD are: no plectin $n = 520$, $c_P/c_K = 0.018$ $n = 161$, $c_P/c_K = 0.06$ $n = 143$, $c_P/c_K = 0.12$ $n = 140$.)

As with potassium the heterogeneity of the network can be tested.²⁰ As already expected, the heterogeneities at plectin ratios of $c_P/c_K = 0.018$ and 0.06 are similar. They all exhibit a heterogeneity of approximately 0.15, representing networks that are very close to but not completely homogeneous. The network with $c_P/c_K = 0.12$ is more heterogeneous and exhibits a value of about 0.19. Thus, plectin shows the same effect as KCl. Increased crosslinker concentrations lead to more heterogeneous networks.

The MSD curves are also used to calculate the dynamic shear modulus, but as with KCl networks, they do not exhibit any special feature (see ESI,† Fig. S2). No plateau modulus G_0 , minima or points of inflection can be seen within the measured regime.

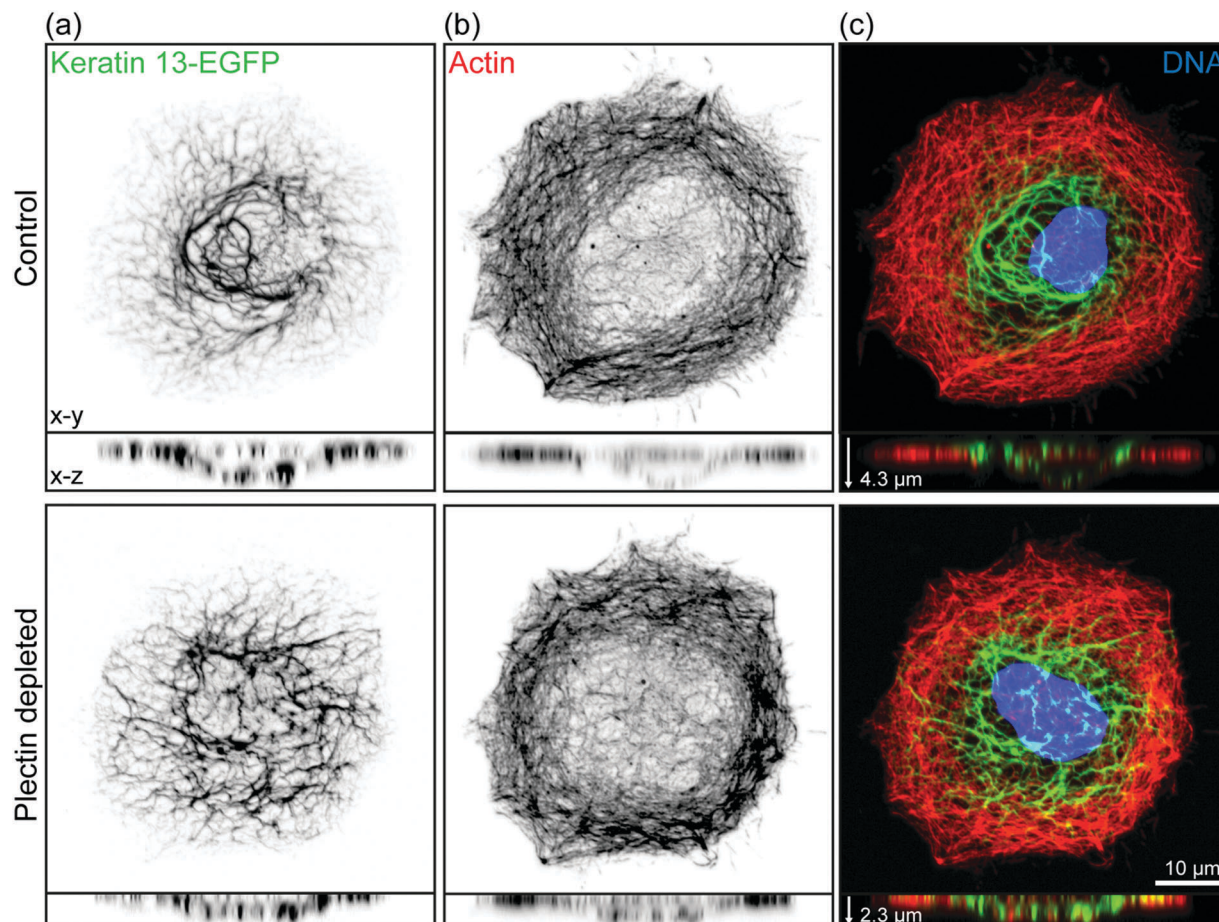


Fig. 5 The fluorescence images show the plectin depleted and control A431 cell clones after membrane extraction. The optical sectioning was done by structured illumination with ApoTome.2 (Carl Zeiss) and the images are maximum intensity projections with the corresponding 2D orthogonal cuts through the middle of the cells. The cells were prepared in the same way as for microrheology experiments prior to fixation in 4% (v/v) PFA. (a) Shows keratin 13-EGFP, (b) F-actin stained with phalloidin, and (c) the composite image of both channels together with Hoechst 33342 stained DNA. The keratin networks are denser around the nucleus and become less pronounced in the cell periphery. Actin behaves *vice versa*: it is more abundant in the peripheral parts of the cell than close to the nucleus.

Effect of plectin on cell networks

The influence of plectin on cells was analyzed in A431 cell clones, where plectin was stably downregulated by shRNA to approximately 10% in comparison to the scramble shRNA control clone, which exhibits normal plectin levels. These single cell clones were generated from the A431 cell line, in detail from the single cell clone AK13-1 that is stably expressing keratin 13-EGFP.²³

After cell extraction keratin and actin networks remained mostly intact in plectin depleted and control cells as shown by fluorescence microscopy in Fig. 5 and for additional cells in Fig. S3 (ESI[†]). Keratin 13 forms thick bundles around the nucleus, while the fluorescent signal decreases towards the cell periphery. In contrast, actin is more abundant in the periphery than close to the nucleus. Formation of stress fibers is in general not very pronounced. There are differences in keratin networks in direct comparison between plectin depleted and control cells after extraction. Keratin filament bundles are slightly thicker in the cell periphery of plectin depleted cells.

Microtubules are dissolved during extraction and thus do not play a role in mechanics measured later. Furthermore, the influence of network stabilization through hemidesmosomes was minimized by cultivation of cells on fibronectin, a substrate that is unfavorable for hemidesmosome formation.²⁴ Staining of integrin- $\beta 4$ showed only a very weak fluorescent signal in both cell clones that was not typical for hemidesmosomal structures (ESI[†], Fig. S4).

Due to the resolution limit of fluorescence microscopy the extracted cells were additionally investigated by scanning electron microscopy (Fig. 6). The left images of Fig. 6((a) and (c)) show an overview of a control cell as well as an image at higher magnification. The right images (Fig. 6(b) and (d)) correspond to plectin depleted cells. The lack of thick keratin bundles, as seen in fluorescence microscopy, can be explained by the rigorous sample preparation protocol for SEM. However, the lower part of the network remains largely intact. Both clones look similar in the overview. The nucleus can still be distinguished, which is surrounded by a three dimensional network. Towards the cell periphery the network collapses on the surface. The images at

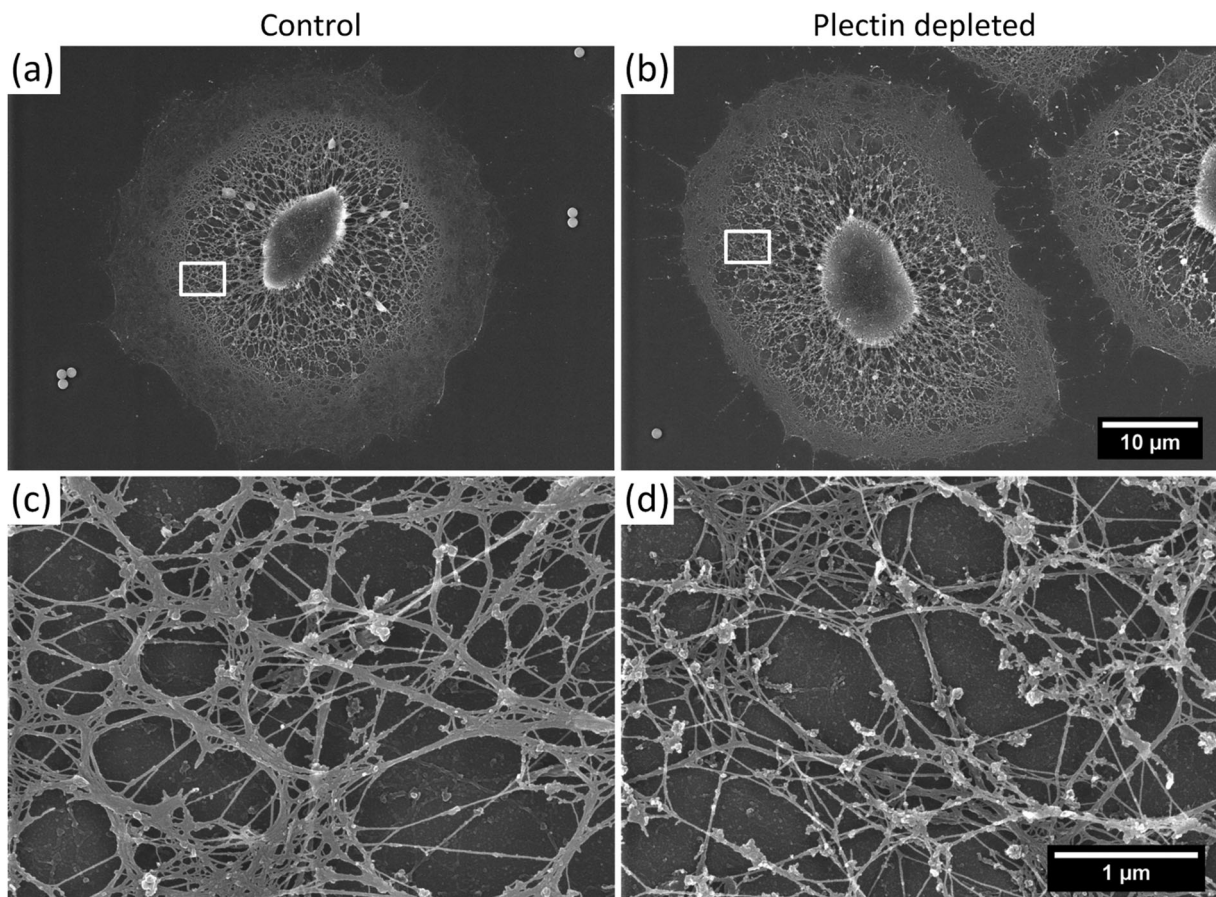


Fig. 6 SEM images of membrane extracted A431 cell clones with normal (a and c) and strongly reduced (b and d) plectin levels (by $\approx 90\%$). For each clone complete cells are shown as well as details of the cytoskeleton (white boxes in the overviews). Higher magnifications reveal more bundling in control cells including normal plectin levels. The thinnest filaments are most likely composed of actin and the slightly thicker filaments are keratins.

higher magnification show thicker bundles in control cells. These data correspond to the proposed role of plectin as a bundling protein,²⁵ but otherwise it cannot be compared to previous studies performed using standard fluorescence microscopy because these methods are not capable of resolving the bundle structure and their exact size. It is also noticeable in both cells that the networks are decorated with small aggregate structures that are probably lipid leftovers from cell extraction.

To measure the local mechanical properties of the intermediate filament network, polystyrene beads were phagocytized by cells before the extraction process. The incubation time of 90 min results in beads that are attached to the network, but not completely incorporated. Thus, the beads have only minimal toxic effects and are furthest away from the substrate. This minimizes the influence of the surface and of possible actin stress fibers which are usually located at the bottom of the cell.²³

From the bead movement within cells again the mean squared displacement is determined. Fig. 7(a) shows the resulting graphs for both cell clones. They exhibit a similar shape when compared to each other, but a different one compared to the other MSDs shown in Fig. 2 and 4. It is much lower than the other curves (even lower than *in vitro* networks including

150 mM KCl) and flatter. Furthermore, saturation occurs, even though no complete plateau is reached. The bead movement is much more restricted than in *in vitro* networks, indicating that the cells are much stiffer.

Compared among each other it can be seen that plectin depleted cells are more flexible than control cells. This is reasonable for a situation where crosslinkers are missing. There seems to be no complete compensation by other cross-linking proteins.

When calculating the heterogeneity, it is observed that cell networks are very inhomogeneous. They have heterogeneity values between 0.4 and 0.45, corresponding to *in vitro* networks including 80 mM KCl. Control cells are slightly more heterogeneous than plectin depleted cells, but the difference is insignificant. Even though the MSDs are similar and both clones are very heterogeneous, the difference between both network types at $\tau = 0.1$ s is significant ($p = 3.9 \times 10^{-24}$).

G' and G'' show that control cells with more crosslinkers are more elastic than plectin depleted cells (Fig. 7(b)). G' approaches a plateau modulus towards lower frequencies for both cell types. It is approximately $G'_{0,\text{control}} = 107$ Pa and $G'_{0,\text{depleted}} = 35$ Pa.

These results are supported by functional deformation assays performed in Boyden chambers with a pore size of 8 μm .

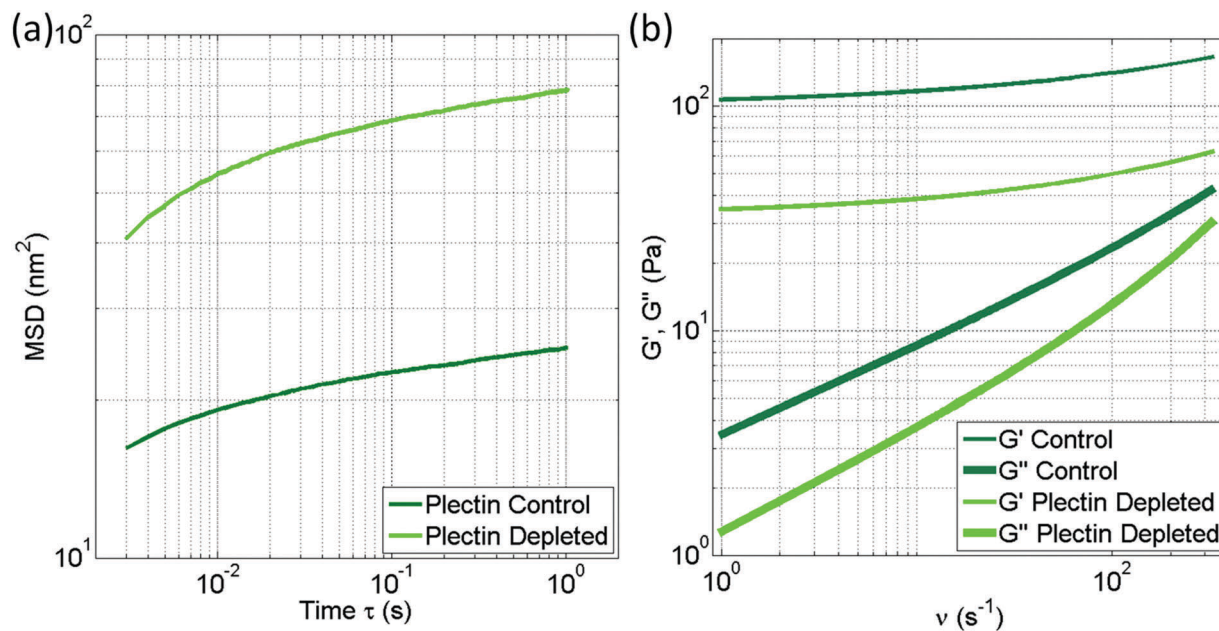


Fig. 7 MSD of plectin depleted and control A431 cells (sampling rate 1000 Hz). Plectin deficient cells result in a higher MSD than control cells (a). Correspondingly, the storage and loss modulus of control cells is higher than in plectin deficient cells (b). (The numbers of beads measured for each MSD are: plectin control $n = 270$, plectin depleted $n = 305$.)

The migration of plectin depleted cells was enhanced by $57\% \pm 25\%$ (6 experiments) compared to control cells.

Discussion

The influence of intermediate filaments on cell rigidity was first investigated by Janmey *et al.*²⁶ They found that vimentin is not very rigid at low strains but hardens at high strains, a behavior important to maintain cell integrity under stress. This was found to be in contrast to actin that is stiffest at low strains but ruptures at high strains. The rigidity of IF networks is not only due to properties of individual filaments, but also due to the interconnection of several filaments and bundle formation. It is shown here that this can either be accomplished with salts like KCl or with crosslinking proteins such as plectin.

The influence of magnesium, a divalent counterion, on network rigidity was already examined by several groups with different rheological methods. Lin *et al.*^{27,28} investigated the rheological behavior of vimentin including MgCl_2 , while Leitner *et al.*²⁹ and Pawelzyk *et al.*³⁰ examined keratin K8/K18. All of them showed network stiffening upon MgCl_2 addition. In contrast, monovalent ions do not influence all types of IFs. While Brennich *et al.*¹⁷ did not observe an effect of KCl on vimentin, Bousquet *et al.*³¹ reported a change in network mechanics by addition of NaCl to keratin K5/K14 networks. These differences can be explained due to distinct line charges carried by various intermediate filaments. There is a critical value for the distance between two polyelectrolytes which is needed to allow bundling.³² When this distance is smaller than the filament radius, then no bundling is possible.

An influence of KCl, as well as MgCl_2 , on K8/K18 network architecture was reported by Hémonnot *et al.*¹⁶ They described

increased filament diameters, especially upon addition of magnesium, and bundle formation at sufficient ion concentrations. Diameter changes could not be observed here with SEM; however, drying of samples and platinum coating probably masks this behavior. On the other side, bundle formation could be confirmed. Increasing KCl concentrations lead to gradual, lateral alignment of filaments and then to dense filament bundles. These bundles are connected with each other through bundle branchings and associations as it was also observed in keratinocytes of the cell line SCC-25.³³

However, no specific onset concentrations for bundling could be confirmed. Hémonnot *et al.*¹⁶ reported bundling onsets at approximately 1 mM MgCl_2 and 25 mM KCl. At these concentrations, changes in the signal of small-angle X-ray scattering measurements become significant. Comparison with SEM images (Fig. 1) shows no abrupt transition in the network structure. With a concentration of 40 mM KCl, which is above the onset concentration, still no distinct bundles are observed. In contrast, MSDs (Fig. 2) already show an influence of 10 mM KCl on network mechanics, which is below the bundling onset concentration. The same gradual change in network mechanics was reported by Leitner *et al.*²⁹ for MgCl_2 . Here also concentrations clearly below the onset concentration were sufficient to alter network mechanics. Thus, ions influence network mechanics through their charges before they affect network morphology.

Comparison with networks containing magnesium shows that much more potassium is needed to induce bundle formation. It does not occur at the same bulk ionic strength.²⁹ However, the bundles resulting from KCl are thicker than with MgCl_2 . As is observed with SEM, more filaments are contained within bundles (data not shown).

Between 80 and 150 mM KCl only a minor difference is seen in network mechanics. This is interesting since the network architecture still changes. Even between 150 and 300 mM KCl a change in network structure is found. This might be due to limitations of the measuring technique, since digitalization of the bead movement from images introduces errors. These errors were corrected in the best possible way, but the resulting MSD might still not be perfect. However, if there is truly no influence in network mechanics, it is an interesting concentration range for this because physiological intracellular KCl concentrations are up to 140 mM. Thus, the saturation in mechanics occurs at concentrations slightly below intracellular KCl concentrations. This would give cells the possibility of controlling their stiffness by influencing bundling due to counterions. This can occur in cells for example with the small heat shock protein Hsp27, which binds to filaments and therefore acts as a spacer.^{34,35}

When adding plectin instead of counterions, specific binding instead of shielding of charges occurs. Plectin appears as filament-attached clusters including different numbers of plectin molecules,²² interconnecting various IFs at specific positions. No bundling occurs.

For characterization of network mechanics the amount of plectin present in cells has to be known. The ratio of plectin to vimentin equals 0.29 in rat glioma C6 cells.²² This includes plectin crosslinking IFs among each other as well as to other cytoskeletal components and hemidesmosomes. *In vitro* measurements showed that a ratio between 0.06 and 0.12 is needed to achieve an increase in network mechanics. Thus, between 20% and 40% of the plectin present in cells has to be used for interlinking of IFs to see a contribution to cell rigidity. At $c_p/c_K = 0.12$ the MSD at $\tau = 0.1$ s is decreased to 40% of the value without plectin. However, it has to be considered that in cells plectin is found in form of thin interconnecting strands,⁵⁴ while here it is seen as clusters including several plectin molecules. These clusters are found at cross-over points stabilizing the filament network considerably.²² Thus, the influence of plectin as a crosslinker between IFs in cells is probably less than measured here *in vitro*.

The *in vitro* results are compared to cell networks of control and plectin downregulated cells. The cells were cultivated for 150 min on fibronectin and in the presence of 1 μ m polystyrene beads for 90 min before membrane extraction. These conditions lead to thicker keratin filament bundles in the cell periphery upon plectin downregulation. In accordance, a detailed investigation of fluorescence images from the same cell clones cultivated on laminin-332-rich matrices for 48 h by Moch *et al.*²³ showed that the keratin network mesh size and keratin bundle thickness are increased upon plectin downregulation. In general, these results fit to results found by Osmanagic-Myers *et al.*²⁵ for basal plectin-null keratinocytes that showed thicker keratin bundles and increased actin stress fiber formation without plectin. Both publications also described pronounced actin stress fiber formation upon plectin removal, which were not observed here likely to shorter cultivation times. In this publication we have looked in more detail on the overall filament

bundling with SEM. It is noticeable that the cytoskeletons are altered in comparison to fluorescence images that were taken directly after membrane extraction. The filaments are stretched toward the nucleus and thick filament bundles are missing, also the networks are strongly collapsed on the substrate in the cell periphery. These are artefacts caused by the sample preparation for SEM. However, it is of interest that the cytoskeleton is less bundled in plectin depleted cells. Our results support therefore the role of plectin as a bundling protein for keratins.

For determination of mechanical properties the cell membranes were extracted and only intermediate filaments, actin, nuclear DNA and associated proteins remained. Thus, the movement of the beads, which were used as measuring probes for passive microrheology, was only influenced by IFs and actin. Microtubules were dissociated and hemidesmosomes were not formed due to short cultivation on fibronectin without FCS. The importance of hemidesmosomes concerning cell stability was already examined in detail.³⁶

Measured network mechanics show a significant difference between both clones. The networks without plectin are more flexible by approximately a factor of three, a difference similar to *in vitro* networks with $c_p/c_K = 0.12$. This might lead to the conclusion that this ratio represents the fraction of plectin used for crosslinking of IFs in cells. However, in extracted cells there is also coupling to actin and actin stress fibers which are rigid structures that give stability to IFs. This coupling is also reduced by plectin depletion. In conclusion, the gain in cytoskeleton flexibility explains increased migration of plectin depleted cells through 8 μ m pores. This gain in flexibility can also explain greater nucleus deformation in plectin-null keratinocytes observed by Almeida *et al.*³⁷ Furthermore, it was not tested if other crosslinking proteins were upregulated by plectin depleted cells to compensate the missing influence of plectin. This might lead to network stiffening that is not attributed to plectin. In fact, rigidity measurements performed on living cells (the same clones as used here) with atomic force microscopy and magnetic tweezers did not show a significant difference between control and plectin depleted cells.²³ This could be due to continuous actin and microtubule polymerization in living cells. Another difference in the compared study was the longer cultivation time which led to a more sessile cell phenotype with lower keratin turnover and thicker keratin networks,³⁸ which could possibly increase cell stability.

It also has to be mentioned that IF networks in cells are much stiffer than *in vitro* assembled networks (compare Fig. 2, 4 and 7). While the MSD of *in vitro* networks spans up to 10^5 nm² (Fig. 2 and 4) in the measured time regime, IF networks in cells are below 100 nm² (Fig. 7). There are several reasons for this. The first reason is based on sample geometry and measurements. The measurements on *in vitro* networks were performed several micrometers away from the surface, while the remaining cell networks are very flat and thus the substrate influences the measuring results. Furthermore, while only K8/K18 was assembled *in vitro*, A431 cells also include other IFs which might have a different rigidity than keratin K8 and keratin K18.³⁹ Additionally, the IF concentration *in vitro* is

lower than in cells (*in vitro*: 0.5 g l^{-1} ; *in vivo*:⁴⁰ up to 40 g l^{-1}). And last but not least, in cells there are other crosslinkers in addition to plectin.⁴¹ Therefore, even after the downregulation of plectin there is still a crosslinking activity present that stiffens the network.

However, results on the mechanical properties of cells and cytoskeletal networks have to be considered carefully. Investigation of the influence of plectin on murine myoblasts (desmin networks) and keratinocytes (keratin networks) revealed that different cell types react differently concerning for example cell stiffness.⁴² While myoblasts showed for example reduced cell stiffness, decreased adhesion strength and lower strain energy after plectin knockout, keratinocytes showed the opposite. Another difference in comparison to keratinocytes is described for fibroblasts. For example, fibroblasts form vimentin networks that are attached to focal adhesions by plectin 1f, while in contrast keratinocytes use plectin 1a to attach keratins to hemidesmosomes.⁴³ Thus, the role of plectin is different depending on the tissue, in which the corresponding cells are found, and on the tasks they have to accomplish there.

Conclusions

We have demonstrated that the stiffness of IF networks and thus cell rigidity are controlled at the level of filament–filament association, *i.e.* single filament *versus* filament bundle formation, through shielding of charges by counterions such as potassium, and by crosslinking of individual IFs through the giant cytolinker plectin. An additional molecular mechanism impacting cytoskeleton rigidity is plectin's physical interaction with actin filaments, thereby integrating the IF and the actin filament systems. With these mechanisms, cells are equipped with powerful tools to fine-tune their rigidity and thereby accommodate to external mechanical stresses.

Experimental

Sample preparation of *in vitro* assembled networks

Human keratin K8 and K18 proteins were isolated and purified as described by Herrmann *et al.*⁴⁴ They were stored at $-80 \text{ }^\circ\text{C}$ in 8 M urea. For filament formation first an equimolar mixture of K8 and K18 was dialyzed into 2 mM Tris-HCl buffer, pH 9.0.²⁹ To start the assembly, 20 mM Tris-HCl buffer, pH 7.0, was added in a 1 : 1 ratio. Furthermore, polystyrene beads with 1 μm diameter (SEM: 1 μl of beads (1.05 g ml^{-1}) in 50 μl of assembly solution; passive microrheology: 2 μl of beads in 100 μl of assembly solution; Duke Standards, Thermo Scientific) and different amounts of KCl were included. In addition, plectin, which was isolated and partially purified from rat glioma C6 cells according to Herrmann and Wiche,⁴⁵ was added in amounts as specified in the text. The assembly was performed at 0.5 g l^{-1} of K8/K18 for at least half an hour for microrheology and for 1 h for SEM samples. The MSDs shown in Fig. 2 and 4 mainly include measurements obtained from two to four independently prepared samples for each sample type. The pure keratin

network and cell measurements include more samples. For more details on the microrheology sample preparation see Neckernuss *et al.*⁴⁶

SEM samples were fixed with 2.5% glutaraldehyde (in 0.1 M phosphate buffer with 1% saccharose) for 30 min and contrasted with OsO_4 (2% in PBS) for 10 min. The buffer was substituted with propanol stepwise (30%, 50%, 70%, 90% and 100%; 5 min per step) and then the network was critical point dried at $38 \text{ }^\circ\text{C}$, 80 bar (Critical Point Dryer CPD 030, BalTec). Afterwards, samples were coated with approximately 3.5 nm of platinum (Baf 300, BalTec) and imaged using a Hitachi S-5200 scanning electron microscope.

Cell culture and sample preparation of cells

Plectin depleted cell clone 1 and scramble control clone 1 from the human epidermoid vulvar carcinoma-derived cell line A431 were described in Moch *et al.*²³ In short, plectin was stably downregulated in the first clone by $\approx 90\%$ by shRNA, in comparison to the control clone where plectin was not affected by scramble control shRNA. The cells were grown in DMEM (Life Technologies) and 10% (v/v) fetal calf serum gold (PAA). For passaging, cells were washed shortly with PBS without $\text{Ca}^{2+}/\text{Mg}^{2+}$ (Biochrom) and trypsinized in trypsin/EDTA 0.05%/0.02% (w/v) solution (Biochrom) for ≈ 1 min. The cells were passaged two times per week and all experiments were performed within 8 passages.

Prior to experiments $\approx 50\,000$ cells per cm^2 were seeded in preconditioned medium on 24×24 mm glass cover slips (Menzel-Gläser, Thermo Fisher Scientific) coated with $5 \mu\text{g cm}^{-2}$ fibronectin (Sigma-Aldrich). After 10 min the preconditioned medium was removed and adherent cells were washed two times and incubated further in serum free DMEM. 60 min after seeding 3 μl (1.05 g ml^{-1}) polystyrene beads with 1 μm diameter were added to the cells for 90 min. Cell membranes were extracted, 150 min post cell plating, on ice by washing the cells with PBS without $\text{Ca}^{2+}/\text{Mg}^{2+}$ following incubation in the same solution supplemented with 1% (v/v) Triton X-100 (Sigma-Aldrich). Finally, the solved membranes were removed by washing three times as before, and remaining samples were stored in the same solution for up to 48 h at $4 \text{ }^\circ\text{C}$ prior to experiments. For more details about cell extraction see Beil *et al.*⁴⁷ The preparation of SEM samples was done in the same way as for *in vitro* networks, with the difference that cells were fixed without saccharose for 1 h in 4% (v/v) paraformaldehyde instead of glutaraldehyde. Laminin-332-rich matrices were prepared as described by Moch *et al.*³⁸

Cell motility was investigated in Boyden chambers with a membrane with pore diameters of 8 μm (Neuro Probe). EGF was used as a chemotactic agent at a concentration of 50 nM.

Immunocytochemistry and fluorescence microscopy

Cells in Fig. S4 (ESI[†]) were washed shortly with PBS at $37 \text{ }^\circ\text{C}$ and fixed for 3 min in methanol and for 30 s in acetone at $-20 \text{ }^\circ\text{C}$. In all other instances cells were extracted and fixed in 4% (v/v) paraformaldehyde for 10 min at room temperature. Prior to staining, cells were incubated in blocking buffer (5% (w/v) bovine serum albumin (Sigma-Aldrich) in PBS) for 1 h. Staining

of F-actin was performed by incubation with Alexa Fluor[®] 555-conjugated phalloidin (Invitrogen) at a concentration of 24 units per ml in antibody dilution buffer (1% (w/v) BSA in PBS) for 40 min. Integrin- β 4 staining was performed by incubation with polyclonal rat integrin- β 4 antibodies (BD Pharmingen) for 1 h at a concentration of 10 $\mu\text{g ml}^{-1}$ in antibody dilution buffer, washing for 15 min with PBS, and incubation with Alexa Fluor[®] 555 conjugated secondary goat antibodies (Invitrogen) for 40 min at a concentration of 8 $\mu\text{g ml}^{-1}$ in antibody dilution buffer. Excess of phalloidin or secondary antibodies was removed by washing for 20 min in PBS. After dipping the coverslips into mono-distilled water, the mounting was performed using Mowiol (Carl Roth) on 76 \times 26 mm glass slides (R. Langenbrinck) and the samples were dried overnight at 4 $^{\circ}\text{C}$.

Recordings were performed using 63 \times Plan-Apochromat objectives (1.40-N.A. DIC M27) on two different systems from Carl Zeiss. The image in Fig. S4(c) of the ESI[†] was recorded using a laser scanning confocal microscope (LSM 710 DUO) by excitation with 488/543 nm lasers and at a pinhole of 2 airy units. All other confocal fluorescence images were recorded using a structured illumination microscope (Apotome.2), an Illuminator HXP 120 C as the light source, and an AxioCam MRm camera. Final images were prepared using Fiji distribution of ImageJ 1.51c⁴⁸ and arranged into figures using Adobe Creative Suite 6.

Microrheology

An inverted microscope with oil-immersion objective (Nikon, ApoTIRF, oil immersion, 100 \times , NA = 1.49) was used for high speed video microscopy. Measurements were done with frame rates of 1000 and 5000 Hz (Motion Pro X4, Imaging Solutions GmbH). The field of view was 25 \times 25 μm (256 \times 256 pixels). The bead motion was digitalized using the PolyParticleTracker software⁴⁹ and trajectories in two dimensions were obtained. System vibrations were corrected by subtracting correlated movement from bead trajectories of the same measurement.⁵⁰ The mean squared displacement (MSD) was calculated from the corrected trajectory. An additional correction factor was multiplied to the resulting MSD,⁵¹ because it is possible that beads move in the same direction by chance. Static errors were determined by measuring immobilized beads (method similar to Kowalczyk *et al.*⁵²). Dynamic errors do not play a role with our measurement parameters. Only the first quarter of the MSD was used for further evaluation because of the worse statistics at longer times.

A minimum of 100 particles was tracked for each sample type. The mean MSD including all beads was used to calculate the dynamic shear modulus by fitting a stretched exponential and then transformation of the fit according to Mason.⁵³ This method overcomes the problems introduced by noise when directly using the Mason method.

Acknowledgements

The authors like to thank U. Nolte, I. Repple and S. Rappl for general support in the lab, P. Walther, E. Schmid and R. Kunz from the Central Facility of Electron Microscopy, Ulm University,

for their help with sample preparation for electron microscopy and T. Tourgaidis and T. Wedig from the DKFZ (Molecular Genetics) for the expression and purification of the protein. Furthermore, we thank M. Beil for many helpful discussions. This work was supported by the Baden-Württemberg Stiftung (Kompetenznetz Funktionelle Nanostrukturen A7) and eCOST. H. Herrmann received financial support from the German Research Foundation (DFG, HE 1853/11-1 and FOR 1228).

Notes and references

- H. Herrmann, H. Bär, L. Kreplak, S. V. Strelkov and U. Aebi, *Nat. Rev. Mol. Cell Biol.*, 2007, **8**, 562–573.
- J. Schweizer, L. Langbein, M. A. Rogers and H. Winter, *Exp. Cell Res.*, 2007, **313**, 2010–2020.
- H. Herrmann and U. Aebi, *Annu. Rev. Biochem.*, 2004, **73**, 749–789.
- N. Geisler and K. Weber, *EMBO J.*, 1982, **1**, 1649–1656.
- E. Fuchs and K. Weber, *Annu. Rev. Biochem.*, 1994, **63**, 345–382.
- R. Kirmse, S. Portet, N. Mücke, U. Aebi, H. Herrmann and J. Langowski, *J. Biol. Chem.*, 2007, **282**, 18563–18572.
- I. Martin, A. Leitner, P. Walther, H. Herrmann and O. Marti, *J. Phys. D: Appl. Phys.*, 2015, **48**, 375401.
- S. Portet, *J. Theor. Biol.*, 2013, **332**, 20–29.
- S. Portet, N. Mücke, R. Kirmse, J. Langowski, M. Beil and H. Herrmann, *Langmuir*, 2009, **25**, 8817–8823.
- T. Lichtenstern, N. Mücke, U. Aebi, M. Mauermann and H. Herrmann, *J. Struct. Biol.*, 2012, **177**, 54–62.
- H. Herrmann, M. Häner, M. Brettel, S. A. Müller, K. N. Goldie, B. Fedtke, A. Lustig, W. W. Franke and U. Aebi, *J. Mol. Biol.*, 1996, **264**, 933–953.
- C. L. Leung, K. J. Green and R. K. Liem, *Trends Cell Biol.*, 2002, **12**, 37–45.
- A. Romani and A. Scarpa, *Arch. Biochem. Biophys.*, 1992, **298**, 1–12.
- R. H. Adrian, *J. Physiol.*, 1956, **133**, 631–658.
- M. Lubin, *Nature*, 1967, **213**, 451–453.
- C. Y. Hémonnot, M. Mauermann, H. Herrmann and S. Köster, *Biomacromolecules*, 2015, **16**, 3313–3321.
- M. E. Brennich, S. Bauch, U. Vainio, T. Wedig, H. Herrmann and S. Köster, *Soft Matter*, 2014, **10**, 2059–2068.
- C. Dammann, H. Herrmann and S. Köster, *Isr. J. Chem.*, 2015, DOI: 10.1002/ijch.201400153.
- J. Kayser, H. Grabmayr, M. Harasim, H. Herrmann and A. R. Bausch, *Soft Matter*, 2012, **8**, 8873–8879.
- Y. Tseng, K. M. An and D. Wirtz, *J. Biol. Chem.*, 2002, **277**, 18143–18150.
- F. C. MacKintosh, J. Käs and P. A. Janmey, *Phys. Rev. Lett.*, 1995, **75**, 4425–4428.
- R. Foisner, F. E. Leichtfried, H. Herrmann, J. V. Small, D. Lawson and G. Wiche, *J. Cell Biol.*, 1988, **106**, 723–733.
- M. Moch, R. Windoffer, N. Schwarz, R. Pohl, A. Omenzetter, U. Schnakenberg, F. Herb, K. Chaisaowong, D. Merhof, L. Ramms, G. Fabris, B. Hoffmann, R. Merkel and R. E. Leube, *PLoS One*, 2016, **11**, e0149106.

- 24 J. C. Jones, S. B. Hopkinson and L. E. Goldfinger, *BioEssays*, 1998, **20**, 488–494.
- 25 S. Osmanagic-Myers, M. Gregor, G. Walko, G. Burgstaller, S. Reipert and G. Wiche, *J. Cell Biol.*, 2006, **174**, 557–568.
- 26 P. A. Janmey, U. Euteneuer, P. Traub and M. Schliwa, *J. Cell Biol.*, 1991, **113**, 155–160.
- 27 Y. C. Lin, C. P. Broedersz, A. C. Rowat, T. Wedig, H. Herrmann, F. C. Mackintosh and D. A. Weitz, *J. Mol. Biol.*, 2010, **399**, 637–644.
- 28 Y. C. Lin, N. Y. Yao, C. P. Broedersz, H. Herrmann, F. C. Mackintosh and D. A. Weitz, *Phys. Rev. Lett.*, 2010, **104**, 058101.
- 29 A. Leitner, T. Paust, O. Marti, P. Walther, H. Herrmann and M. Beil, *Biophys. J.*, 2012, **103**, 195–201.
- 30 P. Pawelzyk, H. Herrmann and N. Willenbacher, *Soft Matter*, 2013, **9**, 8871–8880.
- 31 O. Bousquet, L. L. Ma, S. Yamada, C. H. Gu, T. Idei, K. Takahashi, D. Wirtz and P. A. Coulombe, *J. Cell Biol.*, 2001, **155**, 747–753.
- 32 G. S. Manning, *Eur. Phys. J. E: Soft Matter Biol. Phys.*, 2011, **34**, 132.
- 33 S. Nafeey, I. Martin, T. Felder, P. Walther and E. Felder, *J. Struct. Biol.*, 2016, **194**, 415–422.
- 34 M. D. Perng, L. Cairns, P. van den IJssel, A. Prescott, A. M. Hutcheson and R. A. Quinlan, *J. Cell Sci.*, 1999, **112**, 2099–2112.
- 35 J. Kayser, M. Haslbeck, L. Dempfle, M. Krause, C. Grashoff, J. Buchner, H. Herrmann and A. R. Bausch, *Biophys. J.*, 2013, **105**, 1778–1785.
- 36 J. R. McMillan, J. A. McGrath, M. J. Tidman and R. A. Eady, *J. Invest. Dermatol.*, 1998, **110**, 132–137.
- 37 F. V. Almeida, G. Walko, J. R. McMillan, J. A. McGrath, G. Wiche, A. H. Barber and J. T. Connelly, *J. Cell Sci.*, 2015, **128**, 4475–4486.
- 38 M. Moch, G. Herberich, T. Aach, R. E. Leube and R. Windoffer, *Proc. Natl. Acad. Sci. U. S. A.*, 2013, **110**, 10664–10669.
- 39 R. Moll, W. W. Franke, D. L. Schiller, B. Geiger and R. Krepler, *Cell*, 1982, **31**, 11–24.
- 40 X. Feng, H. Zhang, J. B. Margolick and P. A. Coulombe, *J. Invest. Dermatol.*, 2013, **133**, 850–853.
- 41 P. A. Coulombe, O. Bousquet, L. L. Ma, S. Yamada and D. Wirtz, *Trends Cell Biol.*, 2000, **10**, 420–428.
- 42 N. Bonakdar, A. Schilling, M. Sporrer, P. Lennert, A. Mainka, L. Winter, G. Walko, G. Wiche, B. Fabry and W. H. Goldmann, *Exp. Cell Res.*, 2015, **331**, 331–337.
- 43 G. Wiche, S. Osmanagic-Myers and M. J. Castanon, *Curr. Opin. Cell Biol.*, 2015, **32**, 21–29.
- 44 H. Herrmann, L. Kreplak and U. Aebi, *Methods Cell Biol.*, 2004, **78**, 3–24.
- 45 H. Herrmann and G. Wiche, *J. Biol. Chem.*, 1987, **262**, 1320–1325.
- 46 T. Neckernuss, L. K. Mertens, I. Martin, T. Paust, M. Beil and O. Marti, *J. Phys. D: Appl. Phys.*, 2016, **49**, 045401.
- 47 M. Beil, A. Micoulet, G. von Wichert, S. Paschke, P. Walther, M. B. Omary, P. P. Van Veldhoven, U. Gern, E. Wolff-Hieber, J. Eggermann, J. Waltenberger, G. Adler, J. Spatz and T. Seufferlein, *Nat. Cell Biol.*, 2003, **5**, 803–811.
- 48 J. Schindelin, I. Arganda-Carreras, E. Frise, V. Kaynig, M. Longair, T. Pietzsch, S. Preibisch, C. Rueden, S. Saalfeld, B. Schmid, J. Y. Tinevez, D. J. White, V. Hartenstein, K. Eliceiri, P. Tomancak and A. Cardona, *Nat. Methods*, 2012, **9**, 676–682.
- 49 S. S. Rogers, T. A. Waigh, X. Zhao and J. R. Lu, *Phys. Biol.*, 2007, **4**, 220–227.
- 50 J. C. Crocker, M. T. Valentine, E. R. Weeks, T. Gisler, P. D. Kaplan, A. G. Yodh and D. A. Weitz, *Phys. Rev. Lett.*, 2000, **85**, 888–891.
- 51 C. J. Rowlands and P. T. So, *Appl. Phys. Lett.*, 2013, **102**, 021913.
- 52 A. Kowalczyk, C. Oelschlaeger and N. Willenbacher, *Meas. Sci. Technol.*, 2015, **26**, 015302.
- 53 T. G. Mason, *Rheol. Acta*, 2000, **39**, 371–378.
- 54 T. M. Svitkina, A. B. Verkhovskiy and G. G. Borisy, *J. Cell Biol.*, 1996, **135**, 991–1007.